Journal of Power Sources 398 (2018) 201–208

Contents lists available at ScienceDirect

Journal of Power Sources

journal homepage: www.elsevier.com/locate/jpowsour

PdAg@Pd core-shell nanotubes: Superior catalytic performance towards electrochemical oxidation of formic acid and methanol

Lin Huang[a], Jun Yang[a], Min Wu[a], Zhenqing Shi[b], Zhang Lin[b], Xiongwu Kang[a,*], Shaowei Chen[a,c]

[a] Guangzhou Key Laboratory for Surface Chemistry of Energy Materials, Ngew Energy Research Institute, School of Environment and Energy, South China University of Technology, Guangzhou, 510006, China

[b] Guangdong Engineering and Technology Research Center for Environmental Nanomaterials, School of Environment and Energy, South China University of Technology, Guangzhou, Guangdong, 510006, China

[c] Department of Chemistry and Biochemistry, University of California, 1156 High Street, Santa Cruz, CA, 95064, United States

HIGHLIGHTS

- Dissolution of Ag from PdAg alloy nanotubes results in the Pd skin on PdAg.
- The PdAg@Pd core-shell structure is confirmed by CV, STEM-EDX and XPS.
- PdAg@Pd is largely roughed and electrochemical surface area is remarkably enhanced.
- The activity towards oxidation of formic acid and methanol is markedly enhanced.
- The enhanced performance of PdAg@Pd is ascribed to the unique core-shell structure.

ARTICLE INFO

Keywords:
PdAg alloy nanotubes
Electrochemical dissolution
Pd skin
Methanol oxidation
Formic acid oxidation
Synergistic effect

ABSTRACT

The catalytic activity of alloy nanomaterials can be well modulated through the electrochemical dissolution of the more active component from alloy nanomaterials. In this paper, PdAg alloy nanotubes of diverse Pd to Ag ratio are prepared by galvanic displacement electrochemical reaction. The Ag-leached PdAg nanotubes are characterized by cyclic voltammetric scans, high-angle annular dark-field scanning transmission electron spectroscopy, energy dispersive X-ray elemental mapping and X-ray photoelectron spectroscopy measurements and demonstrate the formation of PdAg@Pd core-shell nanotubes structure with roughed surface and largely enhanced electrochemical surface area. The PdAg@Pd core-shell nanotubes show significantly enhanced catalytic activities and durability towards electro-oxidation of formic acid and methanol than the as-prepared PdAg nanotubes, with the mass activity and specific activity of 1.93 A mg^{-1} and 2.67 mA cm^{-2} towards formic acid respectively, which are 7.8 and 4.8 times that of Pd/C. The increased catalytic performance is ascribed to the unique surface and electronic structure of PdAg@Pd core-shell nanotubes.

1. Introduction

Direct small organic molecule (methanol, formic acid, etc.) fuel cells have been attracting extensive attentions owing to their low operating temperature, high energy density and low environmental pollution, which can be served as a promising clean energy source for portable electronic devices and automobiles [1]. As catalyst for anode electrochemical oxidation, especially for formic acid and methanol oxidation, palladium (Pd) is reported to be resistant towards CO poisoning and outperforms Pt [2–7], thus becoming the heart of the research of the anode catalyst. Pd catalysts of diverse morphology at the nanoscale, such as nanoparticles [8], hollow nanospheres [9], nanosheets [10,11], etc. were prepared, and were found that the morphology of the catalyst have significant effect on the electro-catalytic performance [11,12]. Another strategy to tune and enhance the catalytic performance of the catalyst is to forming bimetallic alloy with another metal or core-shell structure with a second metal as core and Pd as shell. For example, PdCu [13], PdCo [14,15], PdNi [16,17], PdPt [18], PdAu [19], PdRu [20], PdAg [21] and PdRh [22], etc. nanomaterials greatly enhanced the mass activity of palladium catalyst, which was ascribed to ligand effect, geometric effect and or ensemble effect [23]. Ligand effect refer to the electronic charge transfer between the two metals atoms, which

* Corresponding author.
E-mail address: esxkang@scut.edu.cn (X. Kang).

https://doi.org/10.1016/j.jpowsour.2018.07.070
Received 23 April 2018; Received in revised form 12 July 2018; Accepted 16 July 2018
0378-7753/

Scheme 1. Schematic illustration (cross-section view) of the as-prepared and dealloyed of PdAg catalyst of the PdAg nanotube.

further resulted in tuning of the electronic structure of the metal catalyst [24]. Geometric effects are aroused by the atomic arrangement of surface atoms that induces compressed and expanded arrangements of surface atoms (strain) [25] (see Scheme 1).

The catalytic activity of alloyed nanomaterials strongly depend on the surface structure [26], which can be well modulated through preferential dissolution of the more electrochemically active component from alloy nanomaterials by chemical or electrochemical reactions [23,27–31]. Strasser and co-workers [27] synthesized the CuPt alloy nanomaterials with Pt-rich surface layers through electrochemical dissolution of Cu from CuPt alloy nanomaterials and significantly enhanced the catalytic activity of the resulting catalyst toward oxygen reduction reaction (ORR), which is 4–6 times that of pure Pt. Further experimental and theoretical studies ascribed such enhanced catalytic activity to the lattice strain of the Pt shell induced by PtCu alloy core, which further shifted the d-band center of the catalyst and also the adsorption energy of the reactants [23].

However, most of the current work taking advantage of electrochemical dissolution are mainly focused on spherical nanoparticles [23,27,28,32–34] at scale of several nanometers, which have quite weak interaction with the substrate, tend to aggregate during catalytic reactions and thus show poor durability. Compared to these spherical nanoparticles, one dimensional (1D) nanowires and nanotubes exhibit prominent merits, such as fewer lattice boundaries and surface defect sites, enhanced electric conductivity and more resistant to dissolution and aggregation [35–39]. Guo and Huang reported the synthesis of hierarchical platinum-cobalt nanowires by featured with platinum-rich, high-index facets, which demonstrated remarkably enhanced catalytic performance towards ORR. Although extensive work has been devoted to engineering the nanostructure of Pt based alloy nanowires and nanotubes to enhance their catalytic activity towards ORR [23,27,40–42], the strategy of electrochemical dissolution, which has been demonstrated as a powerful tool to enhance the catalyst of nanospheres, has been largely ignored to modulate the Pd-based one-dimensional nanomaterials, especially towards electro-oxidation of small organic molecules.

In this work, 1D PdAg alloy nanotubes (NTs) with various Pd to Ag ratio were prepared by galvanic exchange reaction of Ag nanowires with Pd salt and further electrochemical dissolution of Ag from PdAg NTs results in the formation of Pd skin on PdAg core, as evidenced by CV scans, XRD, XPS and STEM-EDX elemental mapping. The catalytic performance of these dealloyed PdAg NTs towards both formic acid and methanol was much enhanced by such electrochemical etching procedure, which is ascribed to the highly roughened surface structure, markedly enhanced electrochemical surface area and the specific activity of PdAg NTs. Eventually, the mass activity and specific activity of the best dealloyed PdAg nanotubes towards formic acid oxidation is 1.93 A mg^{-1} and 2.67 mA cm^{-2} respectively, which are 7.8 and 4.8 times that of Pd/C.

2. Experimental section

2.1. Chemicals and materials

Silver nitrate ($AgNO_3$, 99%, Energy Chemical), sodium tetrachloropalladate ($NaPdCl_4$, 99%, Energy Chemical), poly (vinyl pyrrolidone) (PVP, $M_w \approx 50000$, Energy Chemical), Nafion solution (5 wt% in 1-propanol and water, Alfa Aesar), Pd/C commercial catalyst (10 wt %, Alfa Aesar) were purchased and used as received. Ethylene glycol (EG, 99%), multi-walled carbon nanotubes (MWCNTs, > 97%), formic acid (HCOOH, 78%) and sodium chloride (NaCl, 99%), sulfuric acid, perchloric acid were purchased from Sinopharm Chemical Reagent Co., Ltd., and used directly. Ultra-pure Water was supplied by a Barnstead Nanopure water system (18.2 MΩ cm) in this work.

2.2. Synthesis of hollow Pd_xAg_1 NTs (x = 0.65, 0.52 and 0.41)

The silver nanowires were first prepared by following the modified procedures in prior report [43,44]. Briefly, anhydrate ethylene glycol (10 ml) was poured into a 100-mL flask and heated to 160 °C for an hour. Mixed solution of 0.085 M $AgNO_3$ and 0.13 M PVP in 6 mL ethylene glycol solution were simultaneously injected into the above solution at a rate of approximately 0.15 mL/min. The resulting solution was further vigorously stirred for 40 min at 160 °C to obtain the product of Ag nanowires. The hollow Pd_xAg_1 NTs were synthesized via the galvanic displacement reaction, where x represents the ratio of Pd to Ag. A dispersion of silver nanowires in EG (2 mL) was poured into 100 ml deionized water and refluxed for 8 min before addition of 0.5 mM aqueous Na_2PdCl_4 (188 ml, 120 ml, 87 ml, 53 ml, respectively). The resulting solution was kept stirring at 100 °C for another 30 min and then cooled to room temperature, which was further kept stirring for 5 h. The white AgCl precipitate were dissolved in saturated aqueous NaCl and centrifuged for multiple times, the final products were dried and stored under vacuum. The atomic ratio of Pd to Ag of PdAg NTs was determined to be 0.65, 0.52 and 0.41 by ICP-Mass (as shown in table S1) and thus final products were denoted as $Pd_{0.65}Ag_1$ $Pd0_{.52}Ag_1$ and $Pd_{0.41}Ag_1$.

2.3. Preparation of dealloyed PdAg NTs

1 mg Pd_xAg_1 and 4 mg CNTs were ultra-sonically dispersed in 5 ml ethanol for 20 min to prepare the catalyst ink. Then 10 μL of the catalyst ink was then drop cast onto GC and dried in vacuum chamber for approximately 15 min at room temperature to form a homogeneous catalyst film on GC surface. Finally, 0.5 wt % Nafion in ethanol was cast on top GCE and dried in air naturally. The prepared GC electrode, a platinum foil and a saturated calomel electrode (SCE) were used as working, counter and reference electrode for electrochemical measurements. The dealloyed Pd_xAg_1 was prepared by subjecting the Pd_xAg_1 to repeated potential cycles in nitrogen-saturated 0.5 M H_2SO_4 aqueous solution for 80 cycles with the potential range from −0.24–0.65 V (vs. SCE), which leach Ag from the PdAg alloy and rendering the formation of the Pd-rich PdAg alloy NTs [45]. The detailed CV profiles were available in supporting information (SI).

2.4. Materials characterization

Powder X-ray diffraction (XRD) was operated on Bruker D8 Advance powder X-ray diffractometer (Cu-Kα radiation, λ = 0.154059 nm, 2θ range of 10–90°, scan rate 10° min). High-resolution TEM (HRTEM) equipped with Energy Dispersive X-Ray Spectrometer (EDX) was

carried out on FEI Tecnai G2 F30 S-TIWN. The X-ray photoelectron spectroscopy (XPS) was performed on PHI X-tool instrument (Ulvac-Phi). The component ratio of Pd to Ag was measured on inductively coupled plasma atomic emission spectrometry (ICP-MS, Perkin Elmer Optima-4300DV Spectrometer).

2.5. Electrochemical characterization

All the electrochemical measurements were carried out on a conventional three-electrode system on CHI-650 E electrochemical workstation at room temperature. The as-prepared and dealloyed Pd_xAg_1 NTs were supported on CNTs and used as working electrode with platinum foil and SCE as counter and reference electrode respectively (in acidic solution). In basic solution, Hg\HgO was used as reference electrode. The electrocatalytic performance of Pd/C and PdAg alloy nanomaterial towards FAOR and MOR was investigated in 0.5 M formic acid in 0.5 M $HClO_4$ aqueous solution and in 1.0 M methanol in 0.5 M NaOH aqueous solution respectively. Chronoamperometric (CA) measurement for FAOR and MOR were conducted at 0.2 V (vs. SCE) and −0.1 V (vs. Hg\HgO), respectively.

2.6. Results and discussion

Fig. 1 (A) show the TEM images of $Pd_{0.52}Ag_1$ NTs, where the hollow NT structure can be clearly observed. The lattice fringes of $Pd_{0.52}Ag_1$ NTs were clearly observed in Fig. 1 (B), from which the lattice distances (20 d, d refers to the single lattice distance) were estimated to be about 4.9 nm and 4.7 nm, which were attributed to (111) and (200) reflections of PdAg alloy, respectively. Fig. 1 (C) shows the HAADF-STEM image and STEM-EDX elemental mapping of Pd-L, Ag-L and the overlap of the two elements of $Pd_{0.52}Ag_1$ NT. The uniform distribution of Pd and Ag all over the NT structures indicates the formation of PdAg alloy. TEM images for $Pd_{0.65}Ag_1$ and $Pd_{0.41}Ag_1$ NTs are available in Fig. S1. The PdAg alloy structure can be further verified by powder XRD. As shown in Fig. S2 (A), the diffraction patterns of Pd_xAg_1 (x = 0.65, 0.52, 0.41) are located between that of Pd and Ag. The dominant diffraction peaks of Pd_xAg_1 (x = 0.65, 0.52, 0.41) at around 38.7°, 45.0°, 65.6° and 78.7° were indexed to (111), (200), (220) and (311) facets of face-centered cubic (fcc) of PdAg phase respectively. The lattice parameters of Pd_xAg_1 (x = 0.65, 0.52 and 0.41) (111) reflections were calculated to be 0.4021, 0.4026 and 0.4035 nm and increased linearly with the decrease of Pd content, as detailed in Fig. S2 (B). All these results suggest the formation of PdAg alloy [46].

The electrochemical etching of Pd_xAg_1 are carried out in 0.5 M sulfuric acid aqueous solution in the potential window of −0.24–0.65 V, as shown Fig S3. The cycling potential is slightly lower than the oxidation potential of Pd, thus avoiding the dissolution of Pd from the alloy NTs. The current peak intensity from Ag oxidation gradually decreases in the anodic scans as the potential cycles proceed. The potential cycling is stopped once the current peak of Ag oxidation disappears, which might suggest the complete dissolution of Ag from the surface and the formation of Pd skin on PdAg alloy NTs [23]. It can be seen in Fig. S3 that $Pd_{0.41}Ag_1$ NTs have higher Ag content and thus more CV cycles are needed to sufficiently dissolute the Ag and form Pd skin on the PdAg alloy NTs. The CV scans of the as-prepared and dealloyed $Pd_{0.65}Ag_1$, $Pd_{0.52}Ag_1$ and $Pd_{0.41}Ag_1$ NTs in 0.5 M NaOH (aq.) are examined and depicted in Fig. 2(A) and (B) and (C) respectively. Two well-defined cathodic peaks are observed as-prepared Pd_xAg_1 NTs at around 0.2 V and −0.25 V, which are attributed to the reduction of the oxides of Ag and Pd [47,48] respectively. The current intensity of Ag in relative to that of Pd increases with the Ag content in the PdAg alloy, indicating that larger surface area of Ag on PdAg alloy with higher Ag content. In contrast, the cathodic peaks from reduction of Ag oxide are completely gone and that from the palladium oxides are intensively enhanced, further confirming the complete dissolution of Ag from the surface of PdAg alloy and formation of Pd skin on PdAg alloy.

Fig. 1(D) and (E) show the HRTEM and TEM images of dealloyed $Pd_{0.52}Ag_1$ supported by CNT, where the NTs structure are remarkably coarsened and the inter-space of the NTs structure are almost fully filled with large grains in relative to that of the as-prepared counterpart. From Fig. 1 (E), lattice fringes of (111) and (200) reflections of dealloyed $Pd_{0.52}Ag_1$ (20 d, d refers to the single lattice distance) are calculated to be ca. 4.8 and 4.5 nm, which are apparently narrowed compared to the as-prepared $Pd_{0.52}Ag_1$ NTs (4.9 and 4.7 nm, respectively, as shown in Fig. 1 (B)). Since the lattice distance of Pd is smaller than that of Ag, thus the partial dissolution of Ag from PdAg might result in lattice contraction of PdAg alloy. This is in agreement with our results. The HAADF STEM image and STEM-EDX element distribution in Fig. 1 (F) reveal that Pd-L and Ag-L uniformly distribute over the entire NTs and overlap very well with each other. Most importantly, it

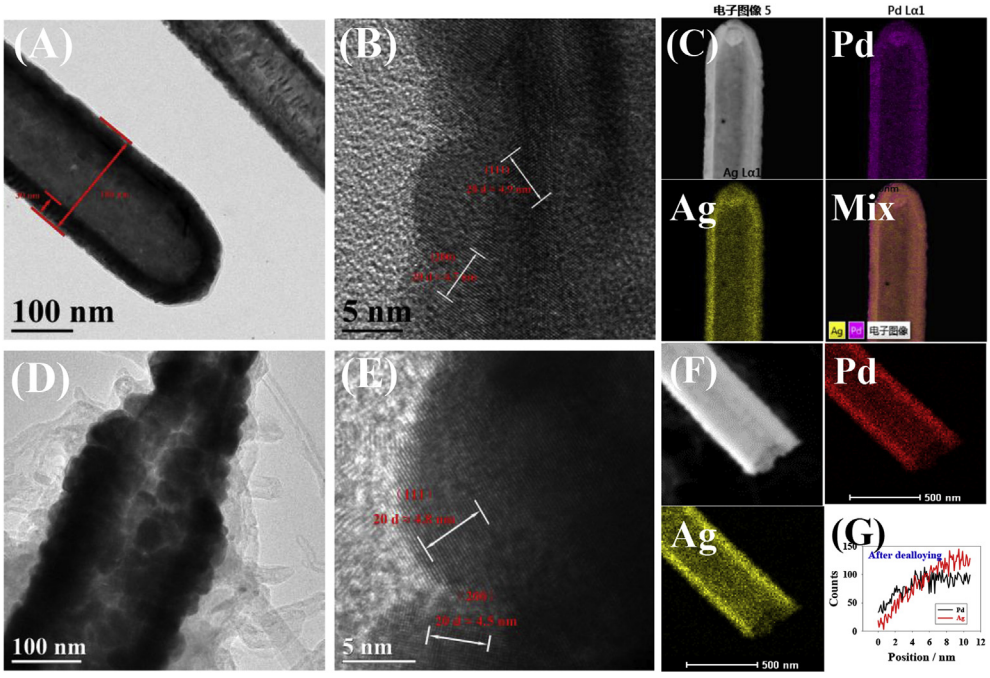

Fig. 1. (A) Low magnification TEM image, (B) HRTEM image and (C) HAAD-STEM image and STEM-EDX elemental mapping for as-prepared $Pd_{0.52}Ag_1$; (D), (E) and (F) are the counterpart characterization for the dealloyed $Pd_{0.52}Ag_1$ supported by CNT. (G) STEM-HAADF line scan of the dealloyed $Pd_{0.52}Ag_1$ supported by CNT, the testing region is marked in Fig. S1 (G).

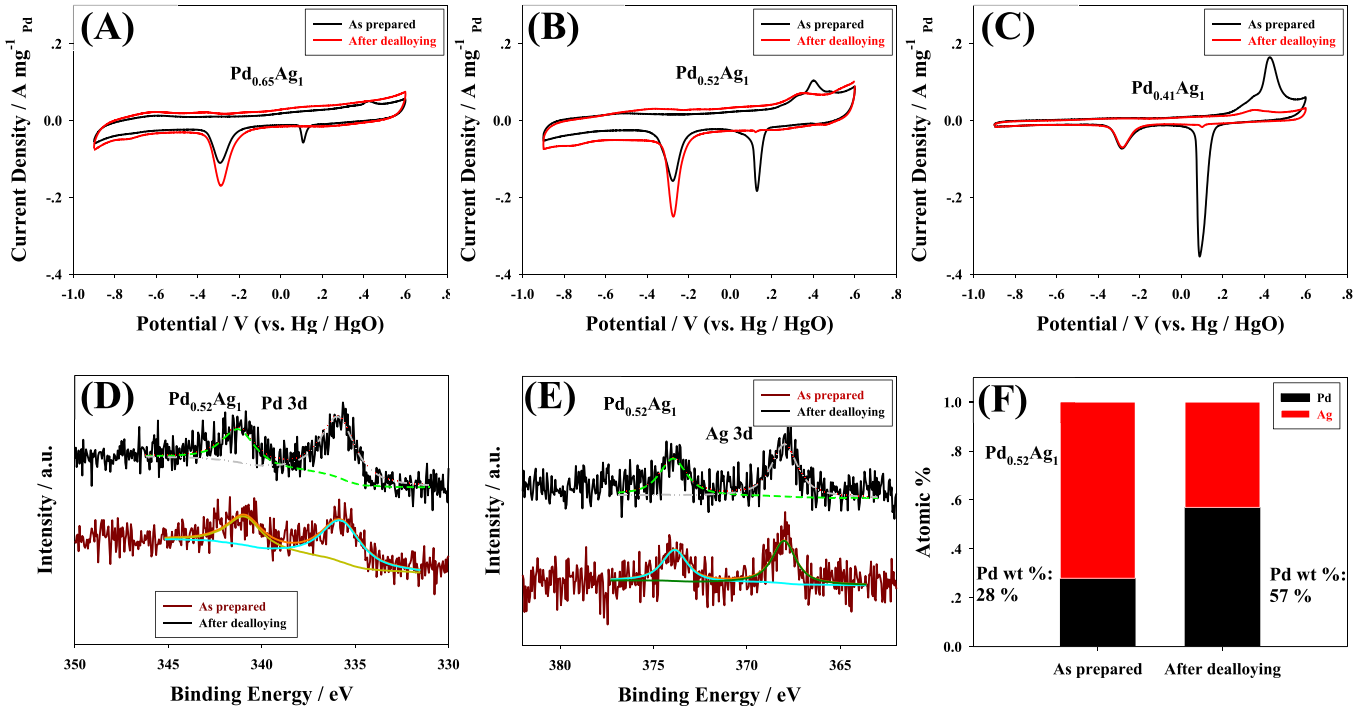

Fig. 2. CV curves of as-prepared and dealloyed PdxAg1/CNTs, x = 0.65(A), 0.52(B) and 0.41(C) in 0.5 M aqueous NaOH solution with scan rate of 100 mV s–1. High-resolution XPS spectra of Pd3d (D) and Ag3d (E) of the as-prepared and dealloyed Pd0.52Ag1, (F) atomic ratio of Pd to Ag of as-prepared and dealloyed Pd0.52Ag1 determined from (E) and (F).

Table 1
The ECSA, mass activity and specific activity of as-prepared and dealloyed Pd_xAg_1 (0.65, 0.52 and 0.41) as well as Pd/C towards FAOR. Δ: Percentage of the enhanced ESCA and catalytic activity by electrochemical dissolution.

samples	ECSA (H_{upd})m^2 g^{-1}		Mass activityA mg^{-1} (Pd)		Specific activitymA cm^{-2}	
	before	after (Δ)	before	after (Δ)	before	after (Δ)
Pd/C	56 ± 4.8		0.32 ± 0.07		0.58 ± 0.09	
$Pd_{0.65}Ag_1$	63 ± 1.3	80 ± 4.1 (38%)	1.36 ± 0.11	1.78 ± 0.05 (31%)	2.16 ± 0.20	2.23 ± 0.07 (3%)
$Pd_{0.52}Ag_1$	66 ± 2.6	94 ± 6.1 (42%)	1.50 ± 0.05	2.52 ± 0.11 (67%)	2.30 ± 0.17	2.67 ± 0.14 (17%)
$Pd_{0.41}Ag_1$	41 ± 1.7	43 ± 2.7 (1%)	0.72 ± 0.13	0.83 ± 0.08 (15%)	1.76 ± 0.19	1.93 ± 0.08 (10%)

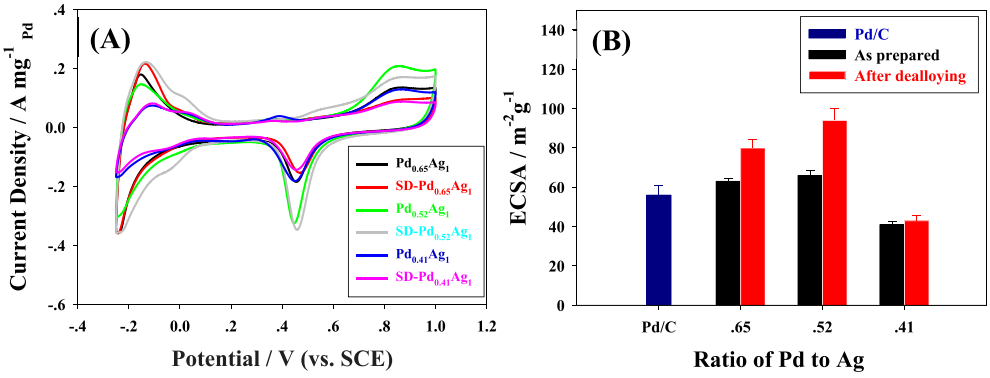

Fig. 3. (A) CV curves and (B) derived ECSA of as-prepared and dealloyed Pd_xAg_1/CNTs (x = 0.65, 0.52, 0.41) in 0.5 M $HClO_4$ aqueous solution at a scan rate of 100 mV s^{-1}.

can be clearly observed that the thickness of the thickness of the Pd shell for PdAg@Pd core-shell structure is about 2 nm from the STEM-HAADF line scan test, as shown in Fig. 1 (G) and Fig. S1 (G). Therefore, it is safe to conclude that the electrochemical dissolution might result in the formation of Pd-rich surface of PdAg alloy structure.

The Pd-rich PdAg alloy NTs derived from electrochemical dissolution is further supported by XPS measurements. Fig. 2(D) and (E) show the high resolution XPS spectra of Pd3d and Ag3d for the as-prepared and dealloyed $Pd_{0.52}Ag_1$. The atomic ratio of Pd to Ag was remarkably enhanced for $Pd_{0.52}Ag_1$ NTs, as shown in Fig. 2 (F). This suggests that

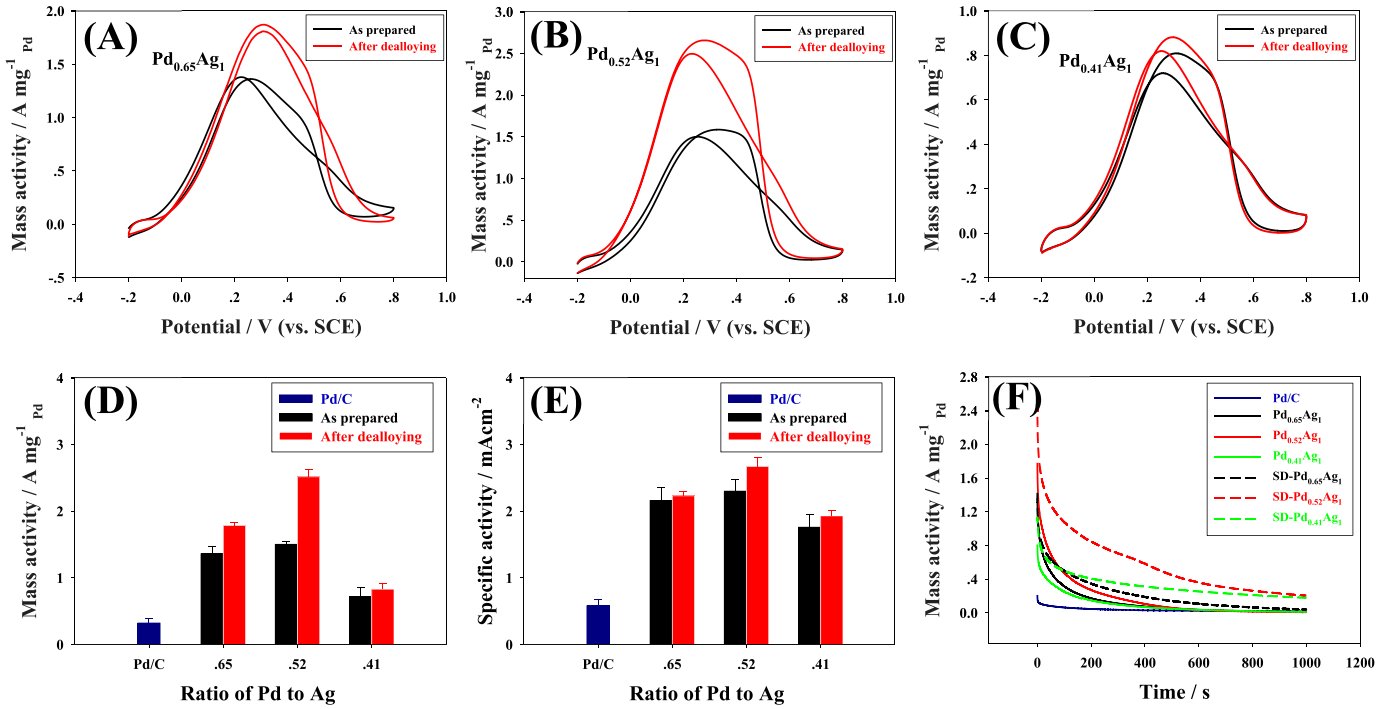

Fig. 4. CV curves of as-prepared and dealloyed Pd_xAg_1/CNTs in 0.5 M formic acid and 0.5 M $HClO_4$, x = 0.65 (A), 0.52 (B) and 0.41(C); mass activity (D), specific activity (E) and i-t measurements for as-prepared and dealloyed Pd_xAg_1/CNTs and Pd/C.

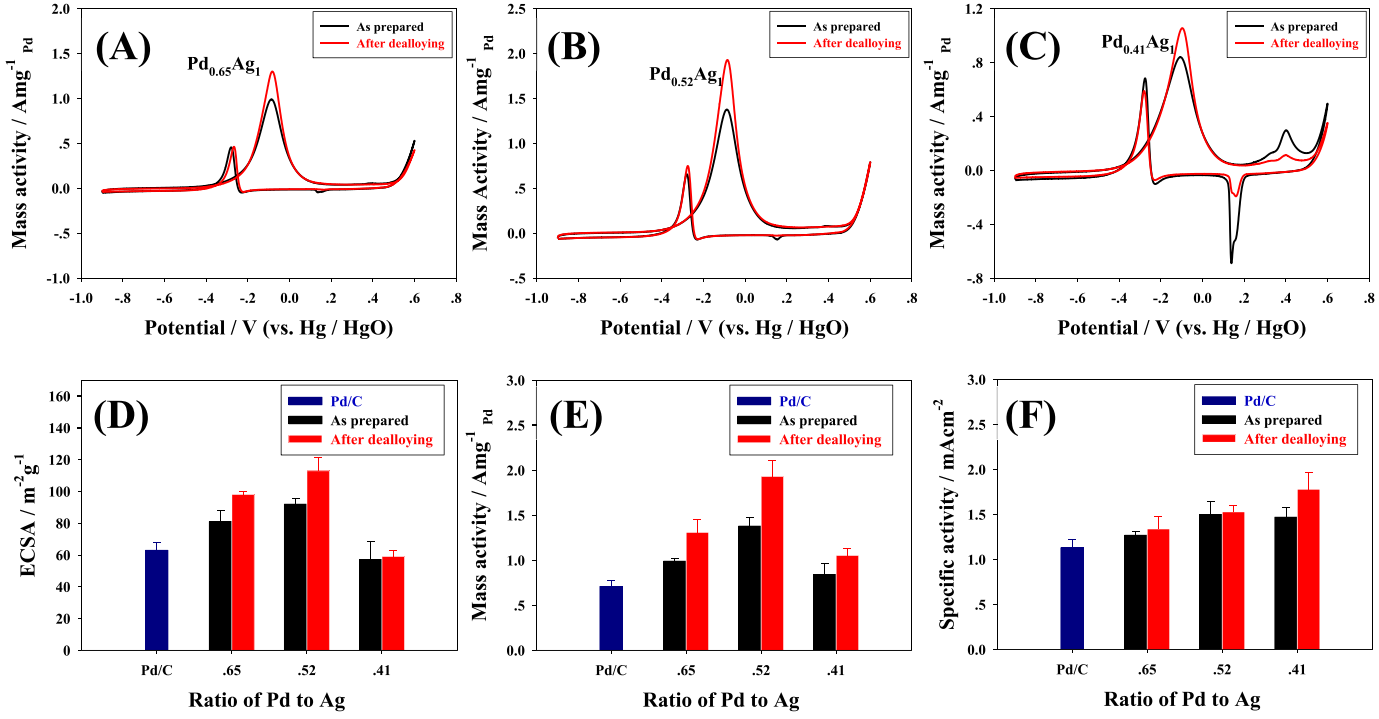

Fig. 5. CV scans of as-prepared and dealloyed Pd_xAg_1, x = 0.65 (A), 0.52 (B), 0.41 (C) in 1.0 M MeOH in 0.5 M NaOH aqueous solution with scan rate of 0.05 mV s^{-1}, ECSA (D), mass activity(E) and specific activity(F) chart of Pd_xAg_1, compared with Pd/C.

electrochemical dissolution of Ag from PdAg alloy mainly occurs on the surface, resulting in the formation of Pd-rich surface structure [23,27,33], in agreement with the electrochemical measurement in Fig. 2(A) and (B) and (C). Similar results are observed for $Pd_{0.65}Ag_1$and $Pd_{0.41}Ag_1$, as shown in Fig. S2. Surprisingly, the binding energy of Pd 3 d (as detailed in Table S2)is reduced upon by electrochemical dissolution, suggesting more electronic donation from Ag to Pd due to the higher electronegativity of Pd than Ag [49]. This might be attributed to the valence electron hybridization and the intra-atomic charge re-distribution [50,51].

3. Electro-catalysis of formic acid oxidation reaction (FAOR)

Fig. 3 (A) show the CV scans of Pd_xAg_1 in 0.5 M $HClO_4$ aqueous solution at a scan rate of 100 mV s^{-1}, from which the electrochemical surface areas (ESCA) are evaluated by under potential hydrogen

Table 2
The ECSA, mass activity and specific activity of as-prepared and dealloyed Pd_xAg_1 (0.65, 0.52 and 0.41) in MOR. Δ: Percentage of the enhanced ESCA and catalytic activity by electrochemical dissolution.

samples	ECSA (PdO) $m^2\ g^{-1}$		Mass activity A mg^{-1} (Pd)		Specific activity mA cm^{-2}		I_f/I_b	
	before	after (Δ)	before	after (Δ)	before	after (Δ)	before	after (Δ)
Pd/C	63 ± 5.0		0.71 ± 0.07		1.13 ± 0.09		3.73	
$Pd_{0.65}Ag_1$	81 ± 7.3	98 ± 2.1 (22%)	0.99 ± 0.03	1.31 ± 0.14 (31%)	1.27 ± 0.04	1.34 ± 0.14 (6%)	2.2	2.8 (27%)
$Pd_{0.52}Ag_1$	92 ± 3.7	126 ± 8.6 (37%)	1.38 ± 0.10	1.93 ± 0.18 (39%)	1.50 ± 0.15	1.53 ± 0.07 (2%)	2.1	2.6 (24%)
$Pd_{0.41}Ag_1$	57 ± 11.3	59 ± 4.1 (3%)	0.84 ± 0.13	1.05 ± 0.08 (25%)	1.47 ± 0.11	1.78 ± 0.19 (21%)	1.3	1.8 (38%)

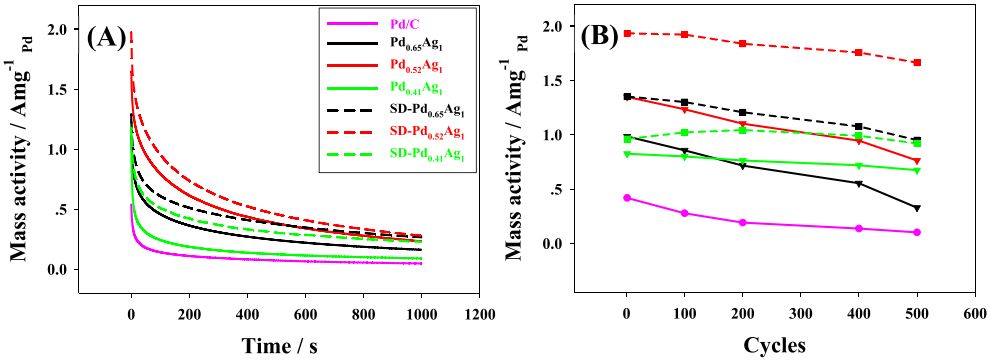

Fig. 6. (A) Chronoamperometric test at −0.1 V and (B) the cycling stability in the potential window of −0.9 to 0.6 V at a scan rate of 0.05 V/s for Pd/C, as-prepared and dealloyed Pd_xAg_1 (x = 0.65, 0.52 and 0.41) in 0.5 M NaOH and 1.0 M MeOH aqueous solution.

desorption (H_{upd}) in −0.2 to 0.12 V [52]. The potential window between 0.12 V and 0.26 V can be attributed to the double-layer charging region [53]. The current peak at about 0.4 V in the anodic scan of the as-prepared PdAg NTs corresponds to the Ag oxidation and vanished after electrochemical dissolution. The cathodic current peaks at about 0.43 V are associated with the reduction of Pd oxides. The ECSA for Pd/C, as-prepared and dealloyed Pd_xAg_1 NTs (x = 0.65, 0.52, 0.41) are shown in Table 1. It can be seen that the ECSA of Pd_xAg_1 NTs is largely increased by electrochemical dissolution. For instance, the ESCA of $Pd_{0.52}Ag_1$ is increased by 42%, changed from 66 ± 2.6 to 94 ± 6.1 m^2g^{-1}. Such increased ECSA of the dealloyed Pd_xAg_1 NTs might be attributed to the roughed structure and the formation of Pd skin on Pd_xAg_1 NTs, consistent with the results of TEM and XPS measurements.

Fig. 4(A) and (B) and (C) display the CVs of the as-prepared and dealloyed Pd_xAg_1 NTs (x = 0.65, 0.52 and 0.41) in 0.5 M HCOOH in 0.5 M $HClO_4$ aqueous solution at a scan rate of 0.05 V s^{-1} respectively and the CV scan of Pd/C are shown in Fig. S5. All the detailed catalytic performance is listed in Table 1. It can be seen that the as-prepared and dealloyed Pd_xAg_1 NTs demonstrate much higher catalytic activity towards formic acid oxidation than Pd/C. Among them, $Pd_{0.52}Ag_1$ NTs exhibits the highest mass activity and specific activity (1.50 ± 0.05 A mg^{-1} and 2.3 ± 0.17 mA cm^{-2}), which is 4.7 and 4.0 times that of the commercial Pd/C catalysts (0.32 ± 0.07 A mg^{-1} and 0.58 ± 0.09 mA cm^{-2}). Surprisingly, further increase or decrease of Ag content in Pd_xAg_1 NTs results in the decrease of both the mass activity and specific activity of Pd_xAg_1 alloy NTs, and a volcano-shape dependence of the catalytic performance of Pd_xAg_1 alloy NTs is observed on the ratio of Pd to Ag, as shown in Fig. 4(D) and (E). This is in agreement with the volcano-shape dependence of the Bader charge of both bulk and surface Pd atoms of PdAg alloy on the ratio of Pd to Ag, signifying the electrochemical catalytic activity of Pd_xAg_1 NTs might strongly depend on the interatomic charge polarization of Pd and Ag in the PdAg alloy, which can remarkably modulate the adsorption of HCOO* on Pd sites [21]. Furthermore, Ag is more chemical active towards oxidation of adsorbed CO than Pd at low potential. Thus the synergistic effect of Ag may further promote the CO_{ad} oxidation and enhance the tolerance Pd active sites towards CO poisoning [32].

The electrochemical dissolution method remarkably enhanced the catalytic performance of Pd_xAg_1 alloy NTs towards formic acid oxidation. The ESCA for $Pd_{0.65}Ag_1$ and $Pd_{0.52}Ag_1$ is increased by 38% and 42% while that of $Pd_{0.41}Ag_1$ is not changed apparently. The specific activity of dealloyed $Pd_{0.52}Ag_1$/CNT and $Pd_{0.41}Ag_1$/CNT are 2.67 ± 0.14 and 1.93 ± 0.08 mA cm^{-2} respectively, increased by 17% and 10% while that for $Pd_{0.65}Ag_1$/CNT are quite consistent with that of the as-prepared. The enhanced specific activity of $Pd_{0.52}Ag_1$/CNT and $Pd_{0.41}Ag_1$/CNT might be ascribed to the unique structure of $Pd_{0.52}Ag_1$ and $Pd_{0.41}Ag_1$ with the formation of Pd skin on PdAg alloy. The enhanced specific activity of Pd_xAg_1 NTs might be contributed to the electronic, assembly and geometric effect [23,27,32,35]. The leaching of surface Ag may create favorable and highly ordered surface Pd atoms arrangements [23,27] and promote the catalytic reaction kinetics towards formic acid oxidation [23]. The mass activity of dealloyed $Pd_{0.65}Ag_1$, $Pd_{0.52}Ag_1$ and $Pd_{0.41}Ag_1$ are 1.78 ± 0.05, 2.52 ± 0.11 and 0.83 ± 0.08 A mg^{-1}, which are enhanced by 31%, 67% and 15% respectively. Among them, dealloyed $Pd_{0.52}Ag_1$ NTs exhibits both the best mass activity and specific activity, which are 7.9 times and 4.8 times that of Pd/C. The enhanced mass activity of the dealloyed $Pd_{0.52}Ag_1$ and $Pd_{0.41}Ag_1$ NTs come from both the enhanced ECSA due to the roughed surface structure of Pd_xAg_1 alloy NTs and also the enhanced specific activity, while that of $Pd_{0.61}Ag_1$ are mainly ascribed to the enlarged ESCA. Fig. 4 (F) shows the i-t curves of the as-prepared and dealloyed Pd_xAg_1/CNTs (x = 0.65, 0.52 and 0.41) in 0.5 M $HClO_4$ in 0.5 M HCOOH (aq.) at 0.2 V. It can be easily found that dealloyed Pd_xAg_1 exhibit much slower deactivation rate than Pd/C and the as-prepared Pd_xAg_1 NTs, indicating enhanced stability of the catalyst towards formic acid oxidation by electrochemical dissolution.

4. Electro-catalytic methanol oxidation reaction (MOR)

The electrochemical performance of as-prepared and dealloyed Pd_xAg_1 NTs towards methanol oxidation reaction was also performed, as depicted in Fig. 5. Based on the CV scans in alkaline medium in Fig. 3, the ECSA of Pd_xAg_1/CNTs catalysts are estimated by the equation:

$$ECSA = Q_{PdO} / (0.405\,mC\,cm^{-2} \times m_{Pd}) \quad (1)$$

where Q_{PdO} is calculated from the integral area of the reduction peaks of Pd oxides divided by the scan rate. The ESCA, mass activity and specific activity of Pd/C, $Pd_{0.65}Ag_1$/CNTs, $Pd_{0.52}Ag_1$/CNTs and $Pd_{0.41}Ag_1$/CNTs before and after electrochemical dissolution are listed in Table 2. The ESCA of dealloyed $Pd_{0.65}Ag_1$ and $Pd_{0.52}Ag_1$ are increased from 81 to 92 $m^2\,g^{-1}$ to 98 and 126 $m^2\,g^{-1}$, corresponding to an enhancement of 22% and 37%, respectively, while dealloyed $Pd_{0.41}Ag_1$ are the same to that of as-prepared $Pd_{0.41}Ag_1$, quite consistent with those derived from H_{upd} in Table 1.

The catalytic activity of the as-prepared and dealloyed Pd_xAg_1 NTs towards methanol oxidation reaction (MOR) is shown in Fig. 5 and the activities are listed in Table 2. The mass activity of as-prepared Pd_xAg_1 NTs is 0.99 ± 0.03, 1.38 ± 0.10 and 0.84 ± 0.13 A mg^{-1} and the dealloyed Pd_xAg_1 are 1.31 ± 0.14, 1.93 ± 0.18 and 1.05 ± 0.08 A mg^{-1}, increased by 31%, 39% and 25%, respectively. The as-prepared $Pd_{0.52}Ag_1$ exhibited the highest mass activity (1.38 A mg^{-1}), which is about 1.94 times that of Pd/C. The dealloyed $Pd_{0.52}Ag_1$ exhibits the largest mass activity, which is 2.72 times that of Pd/C. No apparent enhancement of the specific activity of dealloyed $Pd_{0.65}Ag_1$ and $Pd_{0.52}Ag_1$ are observed in relative to the as-prepared samples. Thus the enhanced mass activity of $Pd_{0.65}Ag_1$ and $Pd_{0.52}Ag_1$ towards methanol oxidation reaction is mainly due to the enhanced ESCA. However, the specific activity of $Pd_{0.41}Ag_1$ is enhanced by 21%, from 1.47 to 1.78 mA cm^{-2}. Thus, the enhanced mass activity for $Pd_{0.41}Ag_1$ is due to both the enhanced ESCA and specific activity.

It has been reported that the forward peak current (I_f) at −0.1 V is resulted from the oxidation of methanol to CO_2, CO and/or other intermediates [54,55]while the backward current (I_b) at −0.3 V is ascribed to the oxidation of the adsorbed carbonaceous intermediates. Thus I_f/I_b is considered to an important indicator to the tolerance of catalysts to CO poisoning. As listed in Table 2, the I_f/I_b for the dealloyed $Pd_{0.65}Ag_1$/CN, $Pd_{0.52}Ag_1$/CN and $Pd_{0.41}Ag_1$/CN are enhanced by 27%, 24% and 38%, much higher than that of the as-prepared Pd_xAg_1, suggesting that the dealloyed PdAg NTs are more resistant to CO poisoning. The enhanced specific activity of $Pd_{0.41}Ag_1$/CN might be partially contributed by the reduced CO poisoning of Pd sites.

The durability of Pd/C, the as-prepared and dealloyed Pd_xAg_1/CNTs for MOR is further confirmed by the chronoamperometric (CA) tests at −0.1 V and potential cycling from −0.9 to 0.6 V at a scan rate of 0.05 V^{-1} in 0.5 M NaOH + 1.0 M MeOH. As shown in Fig. 6 (A), the CA curves of the dealloyed are much higher than that of Pd/C and the as-prepared Pd_xAg_1/CNTs. It can be seen in Fig. 6 (B) that Pd/C lost most of its activity rapidly and 15% of its initial mass activity are retained after merely 500 cycles while the as-prepared $Pd_{0.65}Ag_1$/CNT, $Pd_{0.52}Ag_1$/CNT and $Pd_{0.41}Ag_1$/CNT retained more than 31%, 54% and 80% of their initial activity respectively after 500 cycles. In striking contrast, the dealloyed Pd_xAg_1 NTs exhibit much enhanced cycling stability, with more than 70%, 86% and 88% of its initial activity retained after 500 cycles.

In summary, PdAg alloy nanotubes of diverse Pd to Ag ratio were prepared by galvanic displacement reaction of Ag nanowires with Pd salt and then further subject to electrochemical dissolution of Ag from PdAg alloy nanotubes in acidic medium. The dealloyed PdAg NTs were further characterized by CV scans, HRTEM, STEM-EDX and XPS measurements and found that the NTs structure was significantly roughed, electrochemical active area markedly enhanced and a Pd skin on PdAg alloy was formed. The catalytic activity of both the as-prepared and dealloyed PdAg NTs towards formic acid and methanol oxidation were studied in details. The dealloyed $Pd_{0.52}Ag_1$ NTs exhibits the best catalytic performance, with ESCA, mass activity and specific activity enhanced by 42%, 67% and 17%. The mass activity and specific activity of $Pd_{0.52}Ag_1$ NTs towards formic acid oxidation are 2.52 A mg^{-1} and of 2.67 mA cm^{-2}, 7.8 and 4.8 times that of Pd/C respectively. $Pd_{0.41}Ag_1$ NTs demonstrated the most enhanced specific activity towards methanol oxidation by electrochemical dissolution, which was enhanced by 21%. The enhanced mass activity of Pd_xAg_1 NTs towards both formic acid and methanol oxidation were be attributed the enlarged surface area and the improved specific activity, while the enhanced specific activity of dealloyed PdAg NTs can be attributed to the unique surface structure of the Pd skin on PdAg alloy and the synergistic effect between Pd and Ag. This work may provide a general strategy to prepare electro-catalysts of high activity and durability.

Notes

The authors declare no competing financial interest.

Acknowledgement

This work was supported by the National Natural Science Foundation of China (No. 51602106), the Fundamental Research Funds for Central Universities (SCUT Grant No. 2017MS066 and 2017MS006). Prof. Z. L. would like to thank the Guangdong Innovative and Entrepreneurial Research Team Program (No. 2016ZT06N569).

Appendix A. Supplementary data

TEM, XRD and XPS characterization of the as-prepared and dealloyed Pd_xAg_1 (x = 0.65.0.52 and 0.41), CV profiles of Pd/C and Ag nanowires towards FAOR and MOR.

Supplementary data related to this article can be found at https://doi.org/10.1016/j.jpowsour.2018.07.070.

References

[1] C. Bianchini, P.K. Shen, Chem. Rev. 109 (2009) 4183–4206.
[2] J.-Y. Wang, H.-X. Zhang, K. Jiang, W.-B. Cai, J. Am. Chem. Soc. 133 (2011) 14876–14879.
[3] L. Feng, J. Chang, K. Jiang, H. Xue, C. Liu, W.-B. Cai, W. Xing, J. Zhang, Nanomater. Energy 30 (2016) 355–361.
[4] S. Chen, H. Su, Y. Wang, W. Wu, J. Zeng, Angew. Chem. Int. Ed. 54 (2015) 108–113.
[5] Y. Jia, Y. Jiang, J. Zhang, L. Zhang, Q. Chen, Z. Xie, L. Zheng, J. Am. Chem. Soc. 136 (2014) 3748–3751.
[6] Y.X. Chen, M. Heinen, Z. Jusys, R.J. Behm, Angew. Chem. Int. Ed. 45 (2006) 981–985.
[7] J. Lović, A. Tripković, S.L. Gojković, K.D. Popović, D. Tripković, P. Olszewski, A. Kowal, J. Electroanal. Chem. 581 (2005) 294–302.
[8] V. Mazumder, S. Sun, J. Am. Chem. Soc. 131 (2009) 4588–4589.
[9] J. Ge, W. Xing, X. Xue, C. Liu, T. Lu, J. Liao, J. Phys. Chem. C 111 (2007) 17305–17310.
[10] X. Qiu, H. Zhang, P. Wu, F. Zhang, S. Wei, D. Sun, L. Xu, Y. Tang, Adv. Funct. Mater. 27 (2017).
[11] X. Huang, S. Tang, X. Mu, Y. Dai, G. Chen, Z. Zhou, F. Ruan, Z. Yang, N. Zheng, Nat. Nanotechnol. 6 (2011) 28–32.
[12] M. Jin, H. Zhang, Z. Xie, Y. Xia, Energy Environ. Sci. 5 (2012) 6352–6357.
[13] Z. Xi, J. Li, D. Su, M. Muzzio, C. Yu, Q. Li, S. Sun, J. Am. Chem. Soc. 139 (2017) 15191–15196.
[14] V. Mazumder, M. Chi, M.N. Mankin, Y. Liu, O.n. Metin, D. Sun, K.L. More, S. Sun, Nano Lett. 12 (2012) 1102–1106.
[15] L.Y. Zhang, Z.L. Zhao, W. Yuan, C.M. Li, Nanoscale 8 (2016) 1905–1909.
[16] C. Du, M. Chen, W. Wang, G. Yin, ACS Appl. Mater. Interfaces 3 (2010) 105–109.
[17] Z. Chen, J. Zhang, Y. Zhang, Y. Liu, X. Han, C. Zhong, W. Hu, Y. Deng, Nanomater. Energy 42 (2017) 353–362.
[18] C. Xu, Q. Hao, H. Duan, J. Mater. Chem. 2 (2014) 8875–8880.
[19] Y. Suo, I.-M. Hsing, Electrochim. Acta 56 (2011) 2174–2183.
[20] K. Miao, Y. Luo, J. Zou, J. Yang, F. Zhang, L. Huang, J. Huang, X. Kang, S. Chen, Electrochim. Acta 251 (2017) 588–594.
[21] D. Liu, M. Xie, C. Wang, L. Liao, L. Qiu, J. Ma, H. Huang, R. Long, J. Jiang, Y. Xiong, Nano Res 9 (2016) 1590–1599.
[22] B.T. Sneed, C.N. Brodsky, C.-H. Kuo, L.K. Lamontagne, Y. Jiang, Y. Wang, F. Tao, W. Huang, C.-K. Tsung, J. Am. Chem. Soc. 135 (2013) 14691–14700.
[23] P. Strasser, S. Koh, T. Anniyev, J. Greeley, K. More, C. Yu, Z. Liu, S. Kaya, D. Nordlund, H. Ogasawara, Nat. Chem. 2 (2010) 454–460.
[24] P. Liu, J.K. Nørskov, Phys. Chem. Chem. Phys. 3 (2001) 3814–3818.
[25] M. Mavrikakis, B. Hammer, J.K. Nørskov, Phys. Rev. Lett. 81 (1998) 2819.
[26] Z.Y. Zhou, Z.Z. Huang, D.J. Chen, Q. Wang, N. Tian, S.G. Sun, Angew. Chem. Int. Ed. 49 (2010) 411–414.
[27] S. Koh, P. Strasser, J. Am. Chem. Soc. 129 (2007) 12624–12625.
[28] C. Wang, M. Chi, D. Li, D. Strmcnik, D. Van der Vliet, G. Wang, V. Komanicky, K.-C. Chang, A.P. Paulikas, D. Tripkovic, J. Am. Chem. Soc. 133 (2011) 14396–14403.

[29] V.R. Stamenkovic, B.S. Mun, K.J. Mayrhofer, P.N. Ross, N.M. Markovic, J. Am. Chem. Soc. 128 (2006) 8813–8819.
[30] Y.-Y. Feng, J.-H. Ma, G.-R. Zhang, G. Liu, B.-Q. Xu, Electrochem. Commun. 12 (2010) 1191–1194.
[31] J. Erlebacher, M.J. Aziz, A. Karma, N. Dimitrov, K. Sieradzki, Nature 410 (2001) 450–453.
[32] Y.Y. Feng, J.H. Ma, G.R. Zhang, G. Liu, B.Q. Xu, Electrochem. Commun. 12 (2010) 1191–1194.
[33] Y. Lu, Y. Jiang, X. Gao, X. Wang, W. Chen, Part. Part. Syst. Char. 33 (2016) 560–568.
[34] R. Jana, A. Bhim, P. Bothra, S.K. Pati, S.C. Peter, Chemsuschem 9 (2016) 2922–2927.
[35] W. Wang, F. Lv, B. Lei, S. Wan, M. Luo, S. Guo, Adv. Mater. 28 (2016) 10117–10141.
[36] M.F. Li, Z.P. Zhao, T. Cheng, A. Fortunelli, C.Y. Chen, R. Yu, Q.H. Zhang, L. Gu, B.V. Merinov, Z.Y. Lin, E.B. Zhu, T. Yu, Q.Y. Jia, J.H. Guo, L. Zhang, W.A. Goddard, Y. Huang, X.F. Duan, Science 354 (2016) 1414–1419.
[37] L.Z. Bu, S.J. Guo, X. Zhang, X. Shen, D. Su, G. Lu, X. Zhu, J.L. Yao, J. Guo, X.Q. Huang, Nat. Commun. 7 (2016).
[38] M.C. Luo, Y.J. Sun, X. Zhang, Y.N. Qin, M.Q. Li, Y.J. Li, C.J. Li, Y. Yang, L. Wang, P. Gao, G. Lu, S.J. Guo, Adv. Mater. (2018) 30.
[39] P.T. Wang, X. Zhang, J. Zhang, S. Wan, S.J. Guo, G. Lu, J.L. Yao, X.Q. Huang, Nat. Commun. 8 (2017).
[40] Y. Huang, T. Zhao, G. Zhao, X. Yan, K. Xu, J. Power Sources 304 (2016) 74–80.
[41] M. Huang, W. Wu, C. Wu, L. Guan, J. Mater. Chem. 3 (2015) 4777–4781.
[42] M. Wang, Y. He, R. Li, Z. Ma, Z. Zhang, X. Wang, Electrochim. Acta 178 (2015) 259–269.
[43] Y. Sun, Y. Xia, J. Am. Chem. Soc. 126 (2004) 3892–3901.
[44] J. Chen, B. Wiley, J. McLellan, Y. Xiong, Z.-Y. Li, Y. Xia, Nano Letters 5 (2005) 2058–2062.
[45] H.F. Yang, Y.Y. Feng, L.X. Du, Z.H. Liu, D. Kong, RSC Adv. 6 (2016) 16904–16910.
[46] Y. Jiang, X. Fan, X. Xiao, T. Qin, L. Zhang, F. Jiang, M. Li, S. Li, H. Ge, L. Chen, J. Mater. Chem. 4 (2016) 657–666.
[47] B. Blizanac, P.N. Ross, N. Marković, J. Phys. Chem. B 110 (2006) 4735–4741.
[48] C. Peng, W. Yang, E. Wu, Y. Ma, Y. Zheng, Y. Nie, H. Zhang, J. Xu, J. Alloy. Comp. 698 (2017) 250–258.
[49] S.K. Sengar, B. Mehta, Govind, Journal of Applied Physics 115 (2014) 124301.
[50] T. Sham, Phys. Rev. B 31 (1985) 1888.
[51] I. Coulthard, T. Sham, Phys. Rev. Lett. 77 (1996) 4824.
[52] Y. Lu, W. Chen, J. Phys. Chem. C 114 (2010) 21190–21200.
[53] V.R. Stamenkovic, B.S. Mun, M. Arenz, K.J. Mayrhofer, C.A. Lucas, G. Wang, P.N. Ross, N.M. Markovic, Nat. Mater. 6 (2007) 241–247.
[54] Y.J. Kang, J.B. Pyo, X.C. Ye, T.R. Gordon, C.B. Murray, ACS Nano 6 (2012) 5642–5647.
[55] Z.Y. Qi, C.X. Xiao, C. Liu, T.W. Goh, L. Zhou, R. Maligal-Ganesh, Y.C. Pei, X.L. Li, L.A. Curtiss, W.Y. Huang, J. Am. Chem. Soc. 139 (2017) 4762–4768.